We are IntechOpen,
the world's leading publisher of
Open Access books
Built by scientists, for scientists

6,900
Open access books available

186,000
International authors and editors

200M
Downloads

Our authors are among the

154
Countries delivered to

TOP 1%
most cited scientists

12.2%
Contributors from top 500 universities

CLARIVATE ANALYTICS
BOOK CITATION INDEX
INDEXED

WEB OF SCIENCE™

Selection of our books indexed in the Book Citation Index
in Web of Science™ Core Collection (BKCI)

Interested in publishing with us?
Contact book.department@intechopen.com

Numbers displayed above are based on latest data collected.
For more information visit www.intechopen.com

Multi-Domain Modelling and Control in Mechatronics: the Case of Common Rail Injection Systems

Paolo Lino and Bruno Maione
Dipartimento di Elettrotecnica ed Elettronica, Politecnico di Bari
Via Re David 200, 70125 Bari,
Italy

1. Introduction

The optimal design of a mechatronic system calls for the proper dimensioning of mechanical, electronic and embedded control subsystems (Dieterle, 2005; Isermann, 1996; Isermann, 2008). According to the current approach, the design problem is decomposed into several sub-problems, which are faced separately, thus leading to a sub-optimal solution. Usually, the mechanical part and the control system are considered independently of each others: the former is designed first, then the latter is synthesized for the already existing physical system. This approach does not exploit many potential advantages of an integrated design process, which are lost in the separate points of view of different engineering domains. The physical properties and the dynamical behaviour of parts, in which energy conversion plays a central role, are not determined by the choices of the control engineers and therefore are of little concern to them. Their primary interests, indeed, are signal processing and information management, computer power requirements, choice of sensors and sensor locations, and so on. So it can happen that poorly designed mechanical parts do never lead to good performances, even in presence of advanced controllers. On the other hand, a poor knowledge of how controllers can directly influence and balance for defects or weaknesses in mechanical components does not help in achieving quality and good performances of the whole process.

Significant improvements to overall system performances can be achieved by early combining the physical system design and the control system development (Isermann, 1996b; Stobart et al., 1999; Youcef-Toumi, 1996). Nevertheless, some obstacles have to be overcome, as this process requires the knowledge of interactions of the basic components and sub-systems for different operating conditions. To this end, a deep analysis considering the system as a whole and its transient behaviour seems necessary. In this framework, simulation represents an essential tool for designing and optimizing mechatronic systems. In fact, it can help in integrating the steps involved in the whole design process, giving tools to evaluate the effect of changes in the mechanical and the control subsystems, even at early stages. Available or suitably built models may be exploited for the geometric optimization of components, the design and test of control systems, and the characterization of new systems.

Since models are application oriented, none of them has absolute validity. Models that differ for complexity and accuracy can be defined to take into account the main physical phenomena at various accuracy levels (Bertram et al., 2003; Dellino et al., 2007b; Ollero et al., 2006). Mathematical modelling in a control framework requires to trade off between accuracy in representing the dynamical behaviour of the most significant variables and the need of reducing the complexity of controller structure and design process. Namely, if all engineering aspects are taken into account, the control design becomes very messy. On the other hand, using virtual prototyping techniques allows characterizing system dynamics, evaluate and validate the effects of operative conditions and design parameters, which is appropriate for mechanical design (Ferretti et al., 2004); nevertheless, despite of good prediction capabilities, models obtained in such a way are completely useless for designing a control law, as they are not in the form of mathematical equations. Instead, from the control engineer point of view, the use of detailed modelling tools allows the safe and reliable evaluation of the control systems.

It is clear that an appropriate modelling and simulation approach cannot be fitted into the limitations of one formalism at time, particularly in the early stages of the design process. Hence, it is necessary a combination of different methodologies in a multi-formalism approach to modelling supported by an appropriate simulation environment (van Amerongen, 2003; van Amerongen & Breedveld, 2003; Smith, 1999). The use of different domain-specific tools and software packages allows to take advantage of the knowledge from different expertise fields and the power of the specific design environment.

In this chapter, we consider the opportunity of integrating different models, at different level of details, and different design tools, to optimize the design of the mechanical and control systems as a whole. The effectiveness of the approach is illustrated by means of two practical case studies, involving both diesel and CNG injection systems for internal combustion engines, which represent a benchmark for the evaluation of performances of the approach. As a virtual environment for design integration, we choose AMESim (Advanced Modelling Environment for Simulation): a simulation tool, which is oriented to lumped parameter modelling of physical elements, interconnected by ports enlightening the energy exchanges between element and element and between an element and its environment (IMAGINE S.A., 2007). AMESim, indeed, is capable of describing physical phenomena with great precision and details and of accurately predicting the system dynamics. In a first step, we used this tool to obtain virtual prototypes of the injection systems, as similar as possible to the actual final hardware. Then, with reference to these prototypes, we also determined reduced order models in form of transfer function and/or state space representations, more suitable for analytical (or empirical) tuning of the pressure controllers. Using virtual prototypes in these early design stages enabled the evaluation of the influence of the geometrical/physical alternatives on the reduced models used for the controller tuning. Then, based on these reduced models, the controller settings were designed and adjusted in accordance with the early stages of the mechanical design process. Finally, the detailed physical/geometric models of the mechanical parts, created by the AMESim package, were exported ad used as a module in a simulation program, which enabled the evaluation of the controllers performances in the closed-loop system. In other words, the detailed simulation models surrogated for a real hardware. Experimental and simulation proved the validity of the proposed approach.

2. Steps in the multi-domain design approach

An integrated design approach gives more degrees of freedom for the optimization of both the mechanical and its control system than the classical approach. In particular, the improvement of the design process could be obtained by considering the following aspects: iteration of the design steps, use of different specific-domains interacting tools for design, application of optimization algorithms supported by appropriate models (Dellino et al., 2007a). The use of different domain-specific tools allows one to take advantage of the knowledge of engineers from different expertise fields and the power of the specific design environment. The interaction during the design process can be realized by using automatic optimization tools and a proper management of communication between different software environments, without the need of the expertise intervention. Instead, the expertise opinion takes place during the analysis phase of performances. The resulting integrated design process could consist in the following steps (Fig. 1):
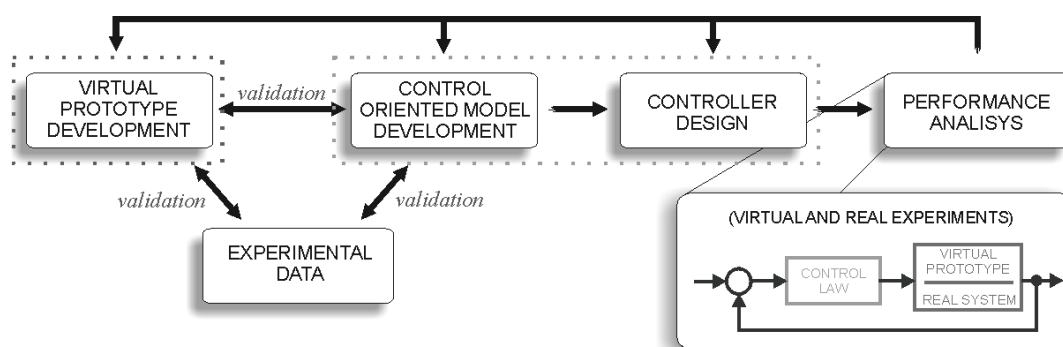

Fig. 1. Integrated design approach for mechatronic systems development.

- Development of a virtual prototype of the considered system using a domain-specific tool (e.g. AMESim, Modelica, etc.) and analysis of the system performances.
- Eventually, realization of a real prototype of the system. Alternatively, a virtual prototype of an existing process can be built and these first two steps have to be swapped.
- Validation of the virtual prototype by comparing simulation results and real data. At the end of this step, the virtual prototype could be assumed as a reliable model of the real system.
- Derivation of a simplified control-oriented analytical model of the real system (white box or black box models). Solving equation of such analytical models is made easier by employing specific software packages devoted to the solution of differential equations (e.g. MATLAB/Simulink).
- Validation of the analytical model against the virtual prototype: this step can be considerably simplified by simulation of different operating conditions.
- Design of control algorithms based on the analytical model parameters. Complex and versatile algorithms are available in computational tools like MATLAB/Simulink to design and simulate control systems. Nevertheless, the construction of accurate models in the same environment could be a complex and stressful process if a deep knowledge of the system under study is not achieved.
- Evaluation of performances of the control laws on the virtual prototype. The use of the virtual prototype allows to perform safer, less expensive, and more reliable tests than

using the real system. In this chapter, the AMESim-Simulink interface allows to integrate AMESim models within the Simulink environment, taking advantage of peculiarities of both software packages.

• The final step consists in evaluating the control algorithm performances on the real system.

The described process could be suitably reiterated to optimize the system and the controller design by using automatic optimization tools. In the next Sections, two case studies involving the common rail injection systems for both CNG and diesel engines are considered to show the feasibility of the described design approach.

3. Integrated design of a compressed natural gas injection system

We consider a system composed of the following elements (Fig. 2): a fuel tank, storing high pressure gas, a mechanical pressure reducer, a solenoid valve and the fuel metering system, consisting of a common rail and four electro-injectors. Two different configurations were compared for implementation, with different arrangements of the solenoid valve affecting system performances (i.e. cascade connection, Fig. 2(a), and parallel connection, Fig. 2(b), respectively). Detailed AMESim models were developed for each of them, providing critical information for the final choice. Few details illustrate the injection operation for both layouts.
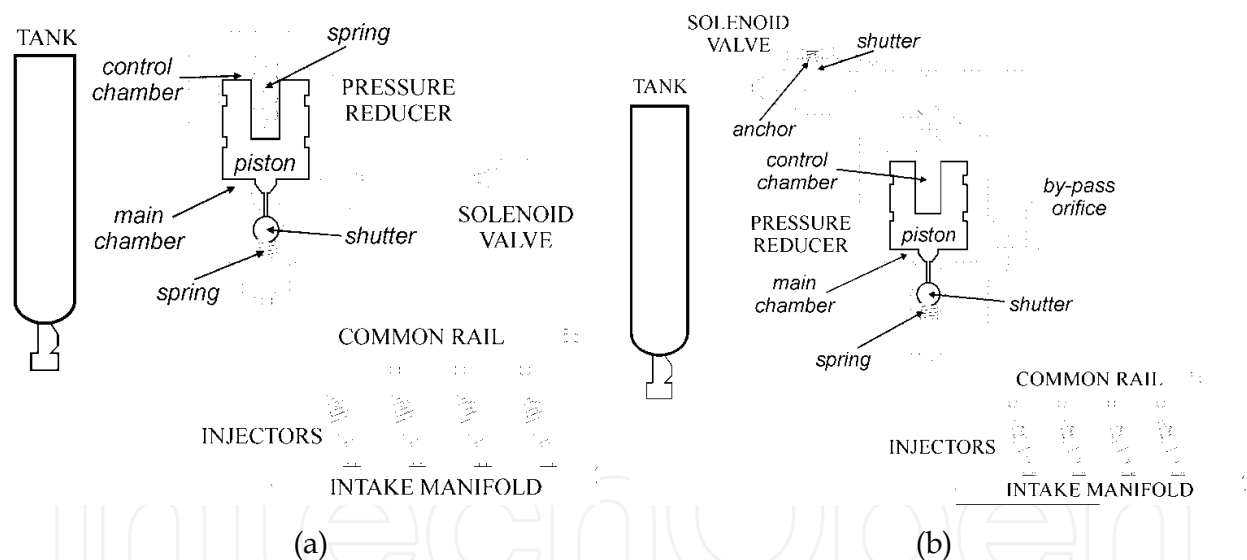

Fig. 2. Block schemes of the common rail CNG injection systems; (a) cascade connection of solenoid valve; (b) parallel connection of solenoid valve.

With reference to Fig. 2(a), the pressure reducer receives fuel from the tank at a pressure in the range between 200 and 20 bars and reduces it to a value of about 10 bar. Then the solenoid valve suitably regulates the gas flow towards the common rail to control pressure level and to damp oscillations due to injections. Finally, the electronically controlled injectors send the gas to the intake manifold for obtaining the proper fuel air mixture. The injection flow only depends on rail pressure and injection timings, which are precisely driven by the Electronic Control Unit (ECU). The variable inflow section of the pressure reducer is varied by the axial displacement of a spherical shutter coupled with a moving

piston. Piston and shutter dynamics are affected by the applied forces: gas pressure in a main chamber acts on the piston lower surface pushing it at the top, and elastic force of a preloaded spring holden in a control chamber pushes it down and causes the shutter to open. The spring preload value sets the desired equilibrium reducer pressure: if the pressure exceeds the reference value the shutter closes and the gas inflow reduces, preventing a further pressure rise; on the contrary, if the pressure decreases, the piston moves down and the shutter opens, letting more fuel to enter and causing the pressure to go up in the reducer chamber (see Maione et al., 2004, for details).

As for the second configuration (Fig. 2(b)), the fuel from the pressure reducer directly flows towards the rail, and the solenoid valve regulates the intake flow in a secondary circuit including the control chamber. The role of the force applied by the preloaded spring of control chamber is now played by the pressure force in the secondary circuit, which can be controlled by suitably driving the solenoid valve. When the solenoid valve is energized, the fuel enters the control chamber, causing the pressure on the upper surface of the piston to build up. As a consequence, the piston is pushed down with the shutter, letting more fuel to enter in the main chamber, where the pressure increases. On the contrary, when the solenoid valve is non-energized, the pressure on the upper side of the piston decreases, making the piston to raise and the main chamber shutter to close under the action of a preloaded spring (see Lino et al., 2008, for details).

On the basis of a deep analysis performed on AMESim virtual prototypes the second configuration was chosen as a final solution, because it has advantages in terms of performances and efficiency. To sum up, it guarantees faster transients as the fuel can reach the common rail at a higher pressure. Moreover, leakages involving the pressure reducer due to the allowance between cylinder and piston are reduced by the lesser pressure gradient between the lower and upper piston surfaces. Finally, allowing intermediate positions of the shutter in the pressure reducer permits a more accurate control of the intake flow from the tank and a remarkable reduction of the pressure oscillations due to control operations. A detailed description of the AMESim model of the system according the final layout is in the following (Fig. 3a).

3.1 Virtual prototype of the compressed natural gas injection system

By assumption, the pressures distribution within the control chamber, the common rail and the injectors is uniform, and the elastic deformations of solid parts due to pressure changes are negligible. The pipes are considered as incompressible ducts with friction and a non uniform pressure distribution. Temperature variations are taken into account, affecting the pressure dynamics in each subcomponent. Besides, only heat exchanges through pipes are considered, by properly computing a thermal exchange coefficient. The tank pressure plays the role of a maintenance input, and it is modelled by a constant pneumatic pressure source. To simplify the AMESim model construction some supercomponents have been suitably created, collecting elements within a single one.

The main components for modelling the pressure reducer are the *Mass block with stiction and coulomb friction and end stops*, which computes the piston and the shutter dynamics through the Newton's second law of motion, a *Pneumatic ball poppet with conical seat*, two *Pneumatic piston*, and an *Elastic contact* modelling the contact between the piston and the shutter.
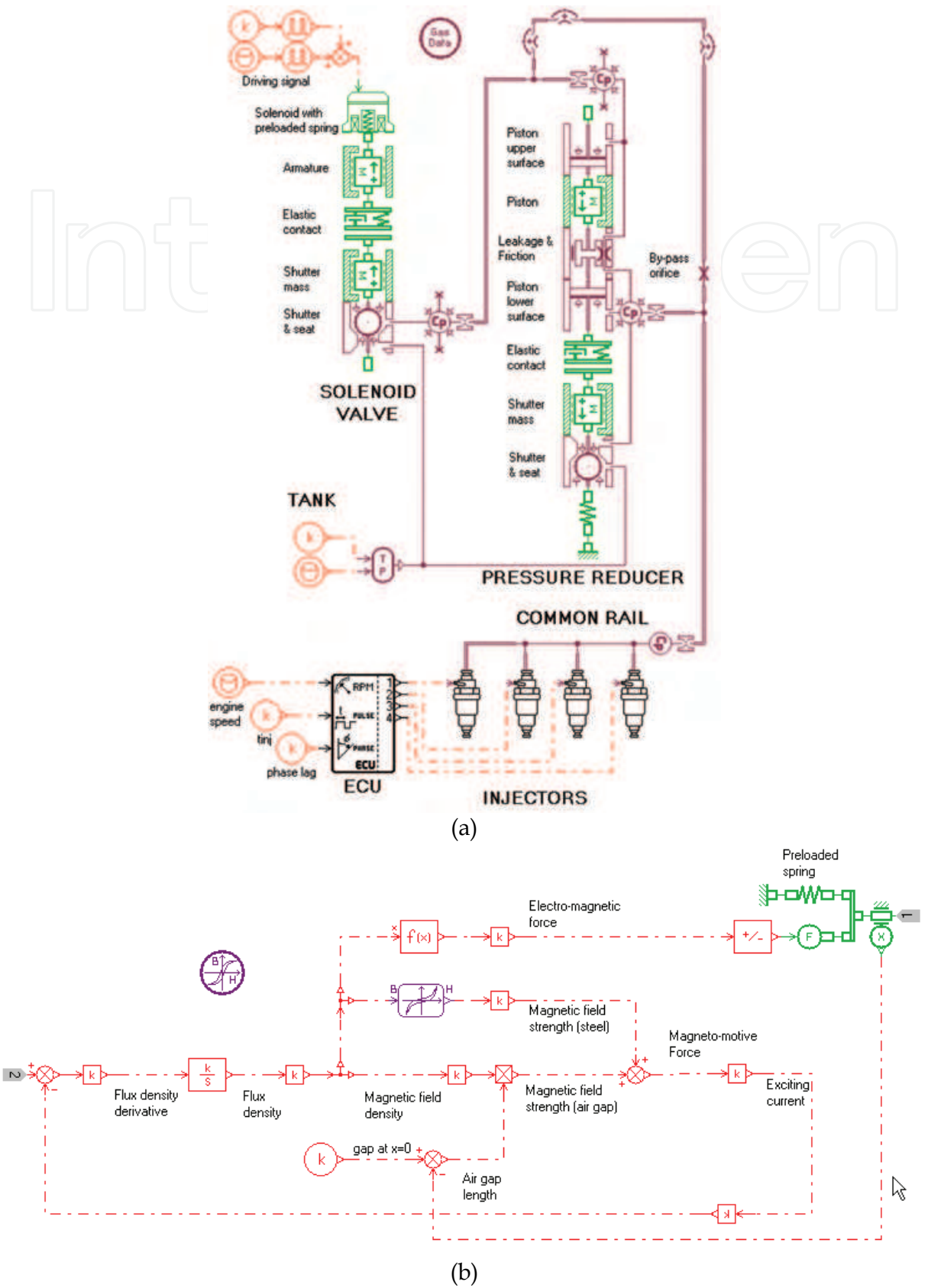
(a)

(b)

Fig. 3. (a) AMESim model of the CNG injection system; (b) solenoid with preloaded spring supercomponent.

The *Pneumatic piston* components compute the pressure forces acting upon the upper and lower piston surfaces. The viscous friction and leakage due to contact between piston and cylinder are taken into account through the *Pneumatic leakage and viscous friction* component, by specifying the length of contact, the piston diameter and the clearance. Finally, a *Variable volume with pneumatic chamber* is used to compute the pressure dynamics as a function of temperature T and intake and outtake flows $\dot{m}_{in}$, $\dot{m}_{out}$, as well as of volume changes due to mechanical part motions, according to the following equation:

$$\frac{dp}{dt} = \frac{RT}{V}\left(\dot{m}_{in} - \dot{m}_{out} + \rho\frac{dV}{dt}\right) \tag{1}$$

where p is the fuel pressure, ρ the fuel density and V the taken up volume. The same component is used to model the common rail by neglecting the volume changes. Both pressure and viscous stresses contribute to drag forces acting on a body immersed in a moving fluid. In particular, the total drag acting on a body is the sum of two components: the pressure or form drag, due to pressure gradient, and the skin friction or viscous drag, i.e. *Drag force = Form drag + Skin friction drag*. By introducing a drag coefficient C_D depending on Reynolds number, the drag can be expressed in terms of the relative speed v (Streeter et al., 1998):

$$Drag = C_D\rho Av^2/2 \tag{2}$$

Moving shutters connecting two different control volumes are subject to both form drag and skin friction drag. The former one is properly computed by AMESim algorithms for a variety of shutters, considering different poppet and seat shapes. As for the latter, it is computed as a linear function of the fluid speed by the factor of proportionality. It can be obtained by noting that for a spherical body it holds *Form Drag = 2πDμv* (Streeter et al., 1998), being μ the absolute viscosity and D the shutter diameter. The moving anchor in the solenoid valve experiences a viscous drag depending on the body shape. The skin friction drag can be computed using eq. (2) by considering the appropriate value of C_D. Since, by hypothesis, the anchor moves within a fluid with uniform pressure distribution, the form drag is neglected.

The continuity and momentum equations are used to compute pressures and flows through pipes so as to take into account wave propagation effects. In case of long pipes with friction, a system of nonlinear partial differential equations is obtained, which is implemented in the *Distributive wave equation submodel of pneumatic pipe* component from the pneumatic library. This is the case of pipes connecting pressure reducer and common rail. The continuity and momentum equations can be expressed as follows (Streeter et al., 1998):

$$\frac{\partial\rho}{\partial t} + \rho\frac{\partial v}{\partial x} = 0 \tag{3}$$

$$\frac{\partial v}{\partial t} + \frac{\alpha^2}{\rho}\frac{\partial\rho}{\partial x} + \frac{f}{2d}v|v| = 0 \tag{4}$$

where α is the sound speed in the gas, d is the pipe internal diameter, f is the D'Arcy friction coefficient depending on the Reynolds number. AMESim numerically solves the above equations by discretization.

For short pipes, the *Compressibility + friction submodel of pneumatic pipe* is used, allowing to compute the flow according the following equation:

$$q = \sqrt{\frac{2d\Delta p}{L\rho f}} \tag{5}$$

where Δp is the pressure drop along the pipe of length L. The pipes connecting common rail and injectors are modelled in such a way.

Heat transfer exchanges are accounted for by the above mentioned AMESim components, provided that a heat transfer coefficient is properly specified. For a cylindrical pipe of length L consisting of a homogeneous material with constant thermal conductivity k and having an inner and outer convective fluid flow, the thermal flow Q is given by (Zucrow& Hoffman, 1976):

$$Q = \frac{2\pi k L \Delta T}{\ln r_o/r_i} \tag{6}$$

where ΔT is the temperature gradient between the internal and external surfaces, and r_o and r_i are the external and internal radiuses, respectively. With reference to the outside surface of the pipe, the heat-transfer coefficient U_o is:

$$U_o = \frac{k}{r_o \ln r_o/r_i} \tag{7}$$

The AMESim model for the solenoid valve is composed of the following elements: a solenoid with preloaded spring, two moving masses with end stops subject to viscous friction and representing the magnet anchor and the shutter respectively, and a component representing the elastic contact between the anchor and the shutter. The intake section depends on the axial displacement of the shutter over the conical seat and is computed within the *Pneumatic ball poppet with conical seat* component, which also evaluates the drags acting on the shutter. The solenoid valve is driven by a peak-hold modulated voltage. The resulting current consists of a peak phase followed by a variable duration hold phase. The valve opening time is regulated by varying the ratio between the hold phase duration and signal period, namely the control signal *duty cycle*. This signal is reconstructed by using a *Data from ASCII file signal source* that drives a *Pulse Width Modulation* component.

To compute the magnetic force applied to the anchor, a supercomponent *Solenoid with preloaded spring* in Fig. 3a modelling the magnetic circuit has been suitably built, as described in the following (Fig. 3b). The magnetic flux within the whole magnetic circuit is given by the Faraday law:

$$\dot{\varphi} = \left(e_{ev} - \mathrm{Re}_v\, i_{ev}\right)/n \tag{8}$$

where φ is the magnetic flux, R the n turns winding resistance, e_{ev} the applied voltage and i_{ev} the circuit current. Flux leakage and eddy-currents have been neglected. The magnetomotive-force *MMF* able to produce the magnetic flux has to compensate the magnetic tension drop along the magnetic and the air gap paths. Even though most of the circuit reluctance is applied to the air gap, nonlinear properties of the magnet, due to saturation and hysteresis, sensibly affect the system behaviour. The following equation holds:

$$MMF = MMF_s + MMF_a = H_s l_s + H_a l_a \qquad (9)$$

where H is the magnetic field strength and l is the magnetic path length, within the magnet and the gap respectively. The air gap length depends on the actual position of the anchor. The magnetic induction within the magnet is a nonlinear function of H. It is assumed that the magnetic flux cross section is constant along the circuit, yielding:

$$B = \varphi/A_m = f(H_s) = \mu_0 H_a \qquad (10)$$

where A_m is the air gap cross section and μ_0 is the magnetic permeability of air. The *B-H* curve is the hysteresis curve of the magnetic material. Arranging the previous equations yields to φ, B and H. The resulting magnetic force and circuit current are:

$$F_{ev} = A_m B^2 \big/ \mu_0 \qquad (11)$$

$$i_{ev} = MMF \big/ n \qquad (12)$$

The force computed by the previous equation is applied to the mass component representing the anchor, so that the force balance can be properly handled by AMESim.
The injectors are solenoid valves driven by the ECU in dependence of engine speed and load. The whole injection cycle takes place in a 720° interval with a 180° delay between each injection. A supercomponent including the same elements as for the solenoid valve has been built to model the electro-injectors. The command signal generation is demanded to the ECU component, which provides a square signal driving each injector and depending on the current engine speed, injector timings and pulse phase angle.

3.2 Controller design for a compressed natural gas injection system

In designing an effective control strategy for the injection pressure it is necessary to satisfy physical and technical constraints. In this framework, model predictive control (MPC) techniques are a valuable choice, as they have shown good robustness in presence of large parametric variations and model uncertainties in industrial processes applications. They predict the output from a process model and then impress a control action able to drive the system to a reference trajectory (Rossiter, 2003). A 2nd order state space analytical model of the plant (Lino et al., 2008) is used to derive a predictive control law for the injection pressure regulation. The model trades off between accuracy in representing the dynamical behaviour of the most significant variables and the need of reducing the computational effort and complexity of controller structure and development. The design steps are summarized in the following. Firstly, the model is linearized at different equilibrium points, in dependence of the working conditions set by the driver power request, speed and load. From the linearized models it is possible to derive a discrete transfer function representation by using a backward difference method. Finally, a discrete Generalised Predictive Contorl (GPC) law suitable for the implementation in the ECU is derived from the discrete linear models equations.
By considering the *duty cycle* of the signal driving the solenoid valve and the rail pressure as the input *u* and output *y* respectively, a family of ARX models can be obtained, according the above mentioned design steps (Lino et al., 2008):

$$\left(1 - a_1 z^{-1}\right) y(t) = \left(b_0 z^{-1} - b_1 z^{-2}\right) u(t) \qquad (13)$$

where z^{-1} is the shift operator and a_1, b_0, b_1 are constant parameters. The j-step optimal predictor of a system described by eq. (13) is (Rossiter, 2003):

$$\hat{y}(t+j\,|\,t) = G_j \Delta u(t+j-1) + F_j y(t) \tag{14}$$

where G_j and F_j are polynomials in q^{-1}, and Δ is the discrete derivative operator. Let $\mathbf{r}$ be the vector of elements $y(t+j)$, $j=1$, ..., N, depending on known values at time t. Then eq. (14) can be expressed in the matrix form $\hat{\mathbf{y}} = \mathbf{G}\tilde{\mathbf{u}} + \mathbf{r}$, being $\tilde{\mathbf{u}} = [\Delta u(t),\dots,\Delta u(t+N-1)]^T$, and $\mathbf{G}$ a lower triangular $N{\times}N$ matrix (Rossiter, 2003).

If the vector $\mathbf{w}$ is the sequence of future reference-values, a cost function taking into account the future errors can be introduced:

$$J = E\left\{ (\mathbf{G}\tilde{\mathbf{u}} + \mathbf{r} - \mathbf{w})^T (\mathbf{G}\tilde{\mathbf{u}} + \mathbf{r} - \mathbf{w}) + \lambda \tilde{\mathbf{u}}^T \tilde{\mathbf{u}} \right\} \tag{15}$$

where λ is a sequence of weights on future control actions. The minimization of J with respect of $\tilde{\mathbf{u}}$ gives the optimal control law for the prediction horizon N:

$$\tilde{\mathbf{u}} = \left(\mathbf{G}^T \mathbf{G} + \lambda I \right)^{-1} \mathbf{G}^T (\mathbf{w} - \mathbf{r}) \tag{16}$$

At each step, the first computed control action is applied and then the optimization process is repeated after updating all vectors. It can be shown (Lino et al., 2008) that the resulting control law for the case study becomes:

$$\Delta u(t) = k_1 w(t) + \left(k_2 + k_3 q^{-1} \right) y(t) + k_4 \Delta u(t-1) \tag{17}$$

where $[k_1, k_2, k_3, k_4]$ depends on N.

4. The common rail injection system of diesel engines

The main elements of the common rail diesel injection system in Fig. 4 are a low pressure circuit, including the fuel tank and a low pressure pump, a high pressure pump with a delivery valve, a common rail and the electro-injectors (Stumpp & Ricco, 1996). Few details illustrate the injection operation. The low pressure pump sends the fuel coming from the tank to the high pressure pump. Hence the pump pressure raises, and when it exceeds a given threshold, the delivery valve opens, allowing the fuel to reach the common rail, which supplies the electro-injectors.

The common rail hosts an electro-hydraulic valve driven by the Electronic Control Unit (ECU), which drains the amount of fuel necessary to set the fuel pressure to a reference value. The valve driving signal is a square current with a variable duty cycle (i.e. the ratio between the length of "on" and the "off" phases), which in fact makes the valve to be partially opened and regulates the rail pressure. The high pressure pump is of reciprocating type with a radial piston driven by the eccentric profile of a camshaft. It is connected by a small orifice to the low pressure circuit and by a delivery valve with a conical seat to the high pressure circuit. When the piston of the pump is at the lower dead centre, the intake orifice is open, and allows the fuel to fill the cylinder, while the downstream delivery valve is closed by the forces acting on it. Then, the closure of the intake orifice, due to the camshaft rotation, leads to the compression of the fuel inside the pump chamber.
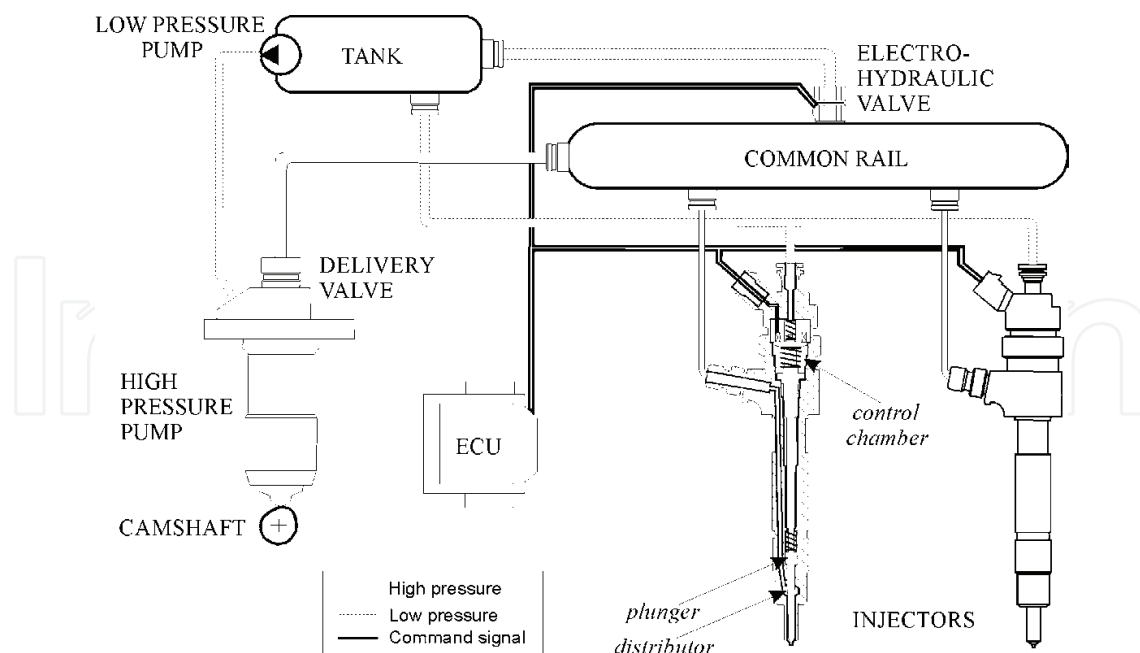
Fig. 4. Block schemes of the common rail diesel injection systems.

When the resultant of valve and pump pressures overcomes a threshold fixed by the spring preload and its stiffness, the shutter of the delivery valve opens and the fuel flows from the pump to the delivery valve and then to the common rail.

As the flow sustained by the high pressure pump is discontinuous, a pressure drop occurs in the rail due to injections when no intake flow is sustained, while the pressure rises when the delivery valve is open and injectors closed. Thus, to reduce the rail pressure oscillations, the regulator acts only during a specific camshaft angular interval (activation window in the following), and its action is synchronized with the pump motion.

The main elements of an electro-injector for diesel engines are a distributor and a control chamber. The control chamber is connected to the rail and to a low pressure volume, and both its inlet and outlet sections are regulated by an electro-hydraulic valve. The distributor includes the feeding pipes and a plunger pushed by a spring against the injection orifices. The plunger axial position depends on the balance of forces acting upon its surfaces, i.e. the control chamber pressure force, the spring force pulling it in closed position, and the distributor pressure force, in the opposite direction. During normal operations the valve electro-magnetic circuit is off and the control chamber is fed by the high pressure fuel coming from the common rail. When the electro-magnetic circuit is excited, the control chamber intake orifice closes while the outtake orifice opens, causing a pressure drop; after a short transient, the plunger reaches the top position disclosing the injection orifices, allowing the injection of the fuel in the cylinders. The Energizing Time (E_T) depends on the fuel amount to be injected. When the electro-magnetic circuit is off the control chamber is filled in, so that the plunger is pulled back by the preloaded spring towards the closed position. In the system under study, the whole injection cycle takes place in a complete camshaft revolution and consists of two injections starting every 180 degrees of rotation.

In the described system, the pressure regulation aims at supplying the engine precisely with the specific amount of fluid and the proper air/fuel mixture demanded by its speed and load.

4.1 Virtual prototype of the common rail diesel injection system

To build the AMESim model for the common rail diesel injection system, similar assumptions than the previous case are made concerning pressure distributions within lumped volumes like common rail, high pressure pump and injectors control volumes. Diversely, temperature does not affect pressure dynamics. Drag forces acting on moving shutters are computed as previously described. Further, the low pressure pump delivers fuel towards the high pressure pump at a constant pressure, so it is considered as an infinite volume source. On the other hand, because of the isobaric expansion during injection, the cylinders' pressure is slightly variable within a range that can be determined experimentally. For this reason, the cylinders are considered as infinite volumes of constant, albeit uncertain, pressure. Since most of the relevant components have been previously described in dept, a brief discussion introduces those used to assemble the virtual prototype of the diesel injection system shown in Fig. 5a. The high pressure pump model is composed of two subsystems, the former representing the pump dynamics, the latter describing the delivery valve behaviour. In particular, the *Cam and cam follower* block is used to represent the cam profile and its rotary motion, which affects the piston axial displacement. The *Spool with annular orifice* models the orifice connecting the low pressure circuit to high pressure pump; its section varies according to the piston displacement. The piston inertia is neglected in this model. The leakage due to contact between piston and cylinder is taken into account through the *Viscous frictions and leakages* component, by specifying the length of contact, the piston diameter and the clearance. Finally, a *Hydraulic volume with compressibility* is used to compute the pressure dynamics as a function of intake and outtake flows q_{in} and q_{out}, as well as of volume changes dm/dt due to mechanical part motions, according to the following equation (IMAGINE S.A., 2007):

$$\frac{dp}{dt} = \frac{K_f}{V}\left(q_{in} - q_{out} - \frac{dm}{dt}\right) \tag{18}$$

where p is the fuel pressure, V the instantaneous volume of liquid and K_f is the fuel bulk modulus of elasticity. The intake and outtake flows come from the energy conservation law.

The same component is used to model the delivery valve internal volume, the control chamber and the distributor volumes inside the electro-injectors, and the common rail.

The components included in the delivery valve model are a *Mass block with stiction and coulomb friction and end stops*, which computes the shutter dynamics, a *Poppet with sharp edge seat*, a *Hydraulic volume with compressibility*, and a *Piston with spring* representing the force applied by the preloaded spring on the delivery valve shutter.

To model pipes within the diesel common rail injection system two situations are considered, i.e. short pipes and long pipes, both accounting for friction, fuel compressibility and expansion of pipes due to high pressures. Short pipes are modelled by the *compressibility + friction hydraulic pipe* sub-model, which uses an effective bulk modulus K_B to take into account both compressibility of the fluid and expansion of the pipe wall with pressure; the effective bulk modulus depends on the wall thickness and Young's modulus for the wall material. The equation describing the pressure dynamics at the mid-point is:

$$\frac{\partial p}{\partial t} + \frac{K_B}{A}\frac{\partial q}{\partial x} = 0 \tag{19}$$
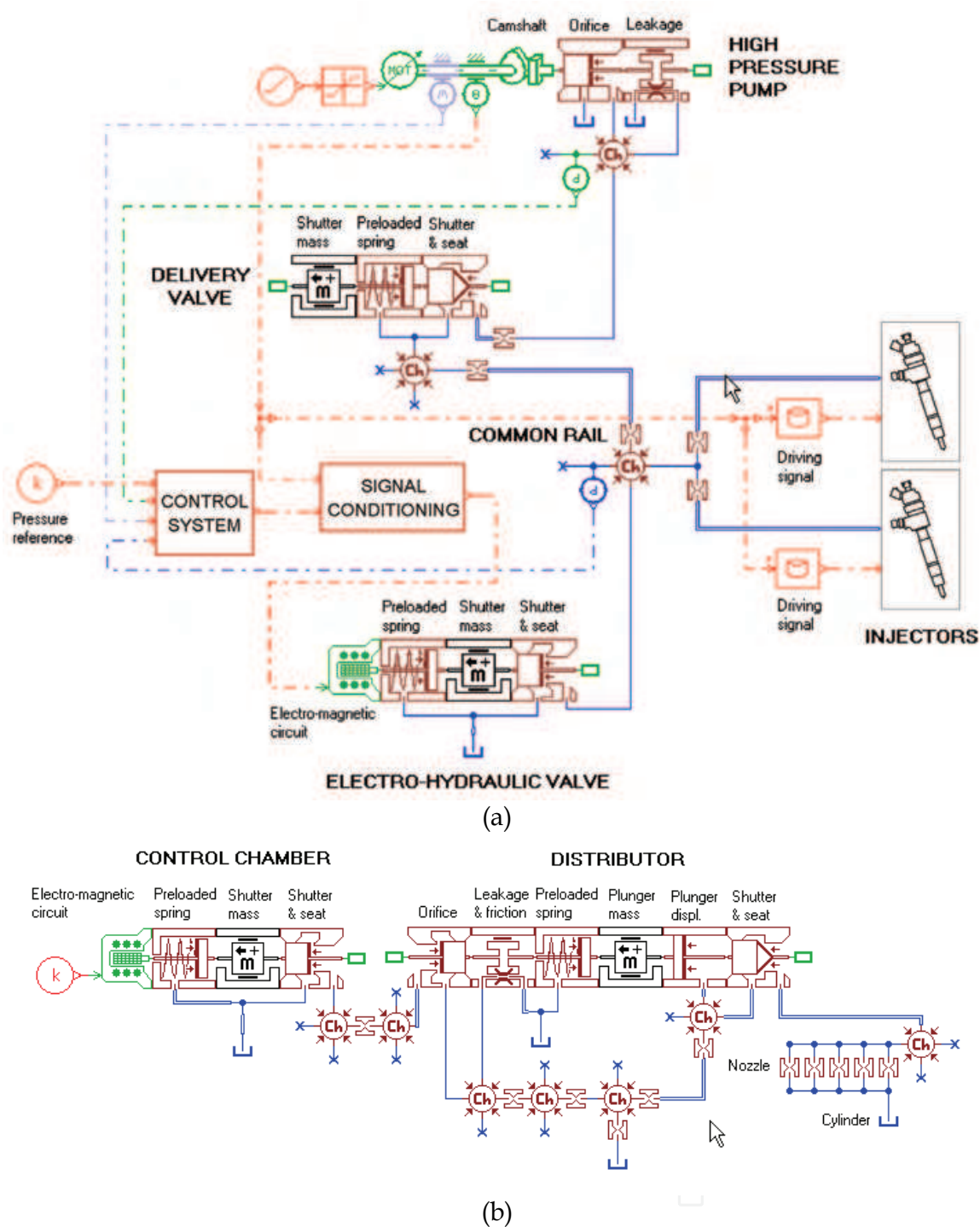
(a)

(b)

Fig. 5. (a) AMESim model of the common rail diesel injection system; (b) Injector supercomponent.

where A is the pressure dependent cross sectional area of pipe. Pipe friction is computed using a friction factor based on the Reynolds number and relative roughness (IMAGINE SA, 2007). The resulting flow is calculated by means of Eq. (5). This model is used for pipes connecting common rail and injectors. The long pipe connecting delivery valve to common rail is modelled by using the *Simple wave equation hydraulic pipe*, which is based on the continuity equation (19) and momentum equation, giving for uncompressible fluids:

$$\frac{\partial q}{\partial t} - \frac{A}{\rho}\frac{\partial p}{\partial x} + v\frac{\partial q}{\partial x} + \frac{f}{2dA}q|q| = 0 \qquad (20)$$

being ρ the fuel density, d the pipe internal diameter, v the mean flow speed and f the friction factor.

The electro-hydraulic valve model includes: a *Mass block with stiction and coulomb friction and end stops* representing the shutter dynamics; a *Piston with spring*; the supercomponent *Electro-magnetic circuit*, which is obtained similarly to the *Solenoid with preloaded spring* supercomponent and converts the controller signal into a force applied to the shutter; a *Spool with annular orifice* modelling the shutter.

Finally, a supercomponent has been used to model the electro-injectors (Fig. 5b), which is a slightly modified version of the block available within the AMESim library. In particular, it consists of two sub-models representing the control chamber and the distributor, respectively. The former sub-model is equal to the electro-hydraulic valve model. The latter includes a *Mass block with stiction and coulomb friction and end stops* and a *Poppet with conical seat* for the plunger, a *Piston with spring*, a *Piston* computing volume changes due to plunger motion, and a *Viscous frictions and leakages* component to take into account flows between the control chamber and the distributor.

4.2 Controller design of the diesel common rail

As previously stated, to develop both an appropriate control strategy and an effective controller tuning a simplified model of the diesel common rail injection system is necessary. In fact, considering too many details and a high number of adjustable parameters make the design of the control law quite difficult. Hence, to this aim, a lumped parameter nonlinear model is considered (Lino et al., 2007), which is suitable for control purposes and can be adapted to different injection systems with the same architecture. The model is validated by simulation, using the package AMESim. The model is expressed in state space form, where the pump pressure p_p and the common rail pressure p_r are the state variables, while the camshaft angular position θ and speed ω_{rpm}, the regulator exciting signal u and the injectors driving signal E_T are the inputs. Assuming, without loss of generality, that no reversal flows occur, the state space representation is (Lino et al., 2007):

$$\begin{aligned} \dot{p}_p &= \eta_a\left(p_p, p_r, \omega_{rpm}, \theta\right) \\ \dot{p}_r &= f_1\left(p_p, p_r\right) + f_2\left(p_r\right)\cdot u + \eta_b\left(p_r, E_T\right) \end{aligned} \qquad (21)$$

where f_1 and f_2 are known functions of pressures, which are accessible for measurement and control. Functions η_a and η_b also depend on parameters which are uncertain (i.e. camshaft angular position and cylinders pressure) and not available for control purpose. The aim of the control action u is to take p_p and p_r close to the constant set-points P_p and P_r. Hence, by defining $e_p = p_p - P_p$ and $e_r = p_r - P_r$, equation (21) become:

$$\begin{aligned} \dot{e}_p &= \eta_a\left(e_p, e_r, \omega_{rpm}, \theta\right) \\ \dot{e}_r &= f_1\left(e_p, e_r\right) + f_2\left(e_r\right)\cdot u + \eta_b\left(e_r, E_{T12}\right) \end{aligned} \qquad (22)$$

Given a system described by equations (22), it is possible to design a sliding mode control law that can effectively cope with system nonlinearities and uncertainties (Khalil, 2002). The

aim of the sliding mode approach is to design a control law u able to take the system trajectory on a sliding surface $s = e_r - \psi(e_p) = 0$ and, as soon as the trajectory lies on this surface, u must also make $e_p = 0$. In (22), e_r plays the role of the control input; therefore the control can be achieved by solving a stabilization problem for $\dot{e}_p = \eta_a(e_p, e_r, \omega_{rpm}, \theta)$. A control law u is designed to bring s to 0 in finite time and to make s maintain this value for all future time. Since by (22)

$$\dot{s} = f_1(e_p, e_r) - \frac{\partial \psi}{\partial e_p} \eta_a(e_p, e_r, \omega_{rpm}, \theta) + f_2(e_r) \cdot u + \eta_b(e_r, E_{T12}) \qquad (23)$$

the control law u can be designed to cancel $f_1(e_p, e_r)$ on the right-hand side of (23):

$$u = \frac{1}{f_2(e_r)}\left[-f_1(e_p, e_r) + \varepsilon\right] \qquad (24)$$

where ε must be chosen to compensate the other nonlinear terms in (23). If the absolute value of the remaining term in (23) is bounded by a positive function $\sigma(e_p, e_r) \geq 0$, it is possible to design ε to force s toward the sliding surface $s = 0$. More precisely, the sliding surface is attractive if ε is given by:

$$\begin{aligned} \varepsilon &= -\beta(e_p, e_r)\text{sgn}(s) \\ \beta(e_p, e_r) &\geq \sigma(e_p, e_r) + \beta_0 \end{aligned} \qquad (25)$$

with $\beta_0 > 0$ coping with uncertainties (Lino et al., 2007). This ensures that $s\dot{s} \leq 0$, so that all the trajectories starting off the sliding surface reach it in finite time and those on the surface cannot leave it. The sliding surface is chosen as $s = e_r + ke_p = 0$, where k is an appropriate constant representing the sliding surface slope. In particular, $e_p \rightarrow 0$ only if $k \rightarrow \infty$. With a finite k, e_p, and consequently e_r, are finite and can only be made smaller than a certain value. However, to avoid saturation of the control valve, k cannot be chosen too high. Finally, the sliding surface is made attractive for the error trajectory by a proper choice of $\beta(e_p, e_r)$. To compensate the rail pressure drop Δp_r caused by the injection occurring within the angular interval [180°, 360°] during regulator inactivity, a compensation term is introduced in the pressure reference which is derived from the injection flow equation. Thus, the new pressure reference becomes $P_r - \Delta p_r$ (Lino et al., 2007).

5. Simulation and experimental results

5.1 The CNG injection system

To assess the effectiveness of the AMESim model in predicting the system behaviour, a comparison of simulation and experimental results has been performed. Since, for safety reasons, air is used as test fluid, the experimental setup includes a compressor, providing air at a constant input pressure and substituting the fuel tank. The injection system is equipped with four injectors sending the air to a discharging manifold. Moreover, a PC system with a National Instrument acquisition board is used to generate the engine speed and load signals, and a programmable MF3 development master box takes the role of ECU driving the injectors and the control valve.

Figure 6 refers to a typical transient operating condition, and compares experimental and simulation results. With a constant 40 bar input pressure, the system behaviour for a

constant t_j = 3ms injectors opening time interval, while varying engine speed and solenoid valve driving signal has been evaluated. The engine speed is composed of ramp profiles (6c), while the *duty cycle* changes abruptly within the interval [2%, 12%] (Fig. 6d). Figures 6a and 6b show that the resulting dynamics is in accordance with the expected behaviour. A maximum error of 10% confirms the model validity.

After the validation process, the AMESim virtual prototype was used to evaluate the GPC controller performances in simulation by employing the AMESim-Simulink interface, which enabled us to export AMESim models within the Simulink environment. The interaction between the two environments operates in a *Normal* mode or a *Co-simulation* mode. As for the former, a compiled S-function containing the AMESim model is generated and included in the Simulink block scheme, and then integrated by the Simulink solver. As for the latter, which is the case considered in this chapter, AMESim and Simulink cooperate by integrating the relevant portions of models.
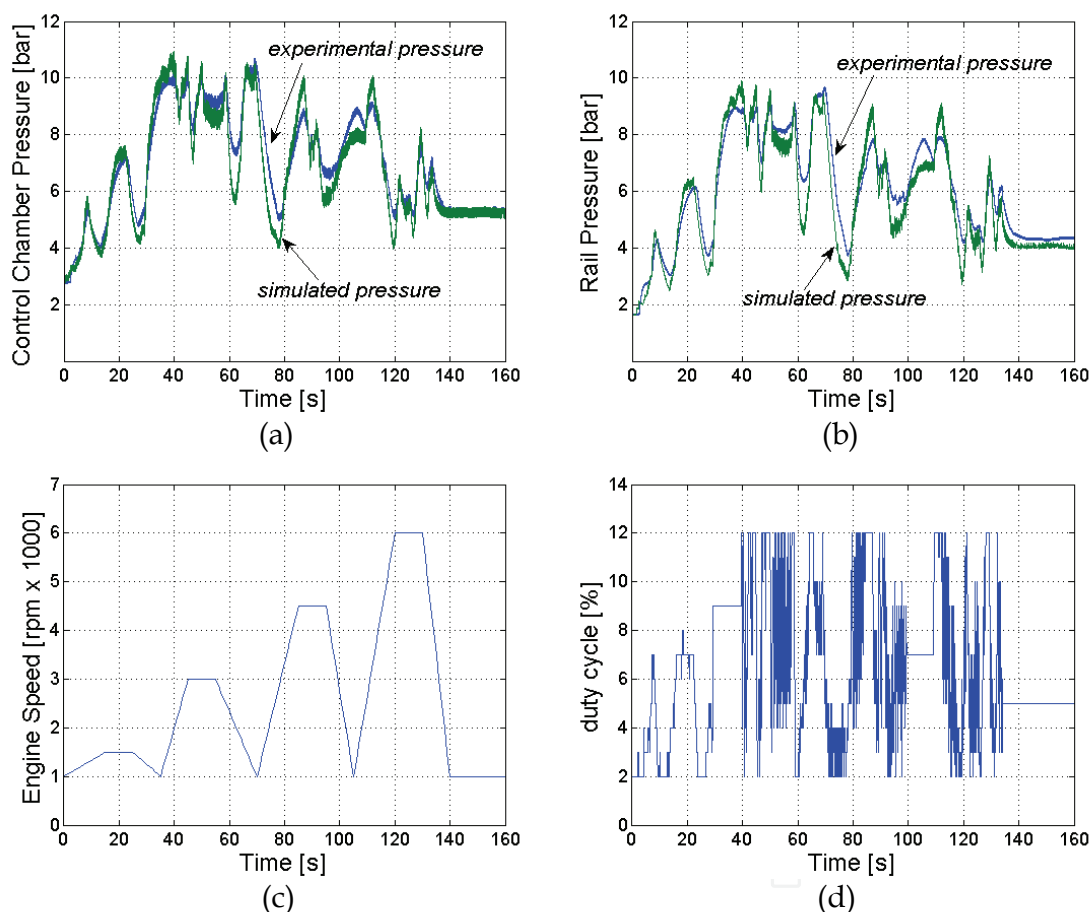
Fig. 6. Simulation and experimental results when varying *duty cycle* and engine speed, with a constant t_j = 3ms; (a) control chamber pressure; (b) common rail pressure; (c) engine speed; (d) control signal *duty cycle*.

The GPC controller was tuned referring to models linearized at the starting equilibrium point, according to design steps of Section 3.2. The test considered ramp variations of the engine speed and load, for the system controlled by a GPC with a $N = 5$ (0.5s) prediction horizon. The input air pressure from the compressor was always 30bar. The rail pressure reference was read from a static map depending on the working condition and had a sort of

ramp profile as well. The final design step consisted in the application of the GPC control law to the real system.

In Fig. 7, the engine speed accelerates from 1100rpm to 1800rpm and then decelerates to 1100rpm, within a 20s time interval (Fig. 7b). The control action applied to the real system guarantees a good reference tracking, provided that its slope does not exceed a certain value (Fig. 7a, time intervals [0, 14] and [22, 40]). Starting from time 14s, the request of a quick pressure reduction causes the control action to close the valve completely (Fig. 7c) by imposing a *duty cycle* equal to 0. Thanks to injections, the rail pressure (Fig. 7a) decreases to the final 5bar reference value, with a time constant depending on the system geometry; the maximum error amplitude cannot be reduced due to the actuation variable saturation. Fig. 7d shows the injectors' exciting time during the experiment. It is worth to note that simulation and experimental results are in good accordance, supporting the proposed approach.
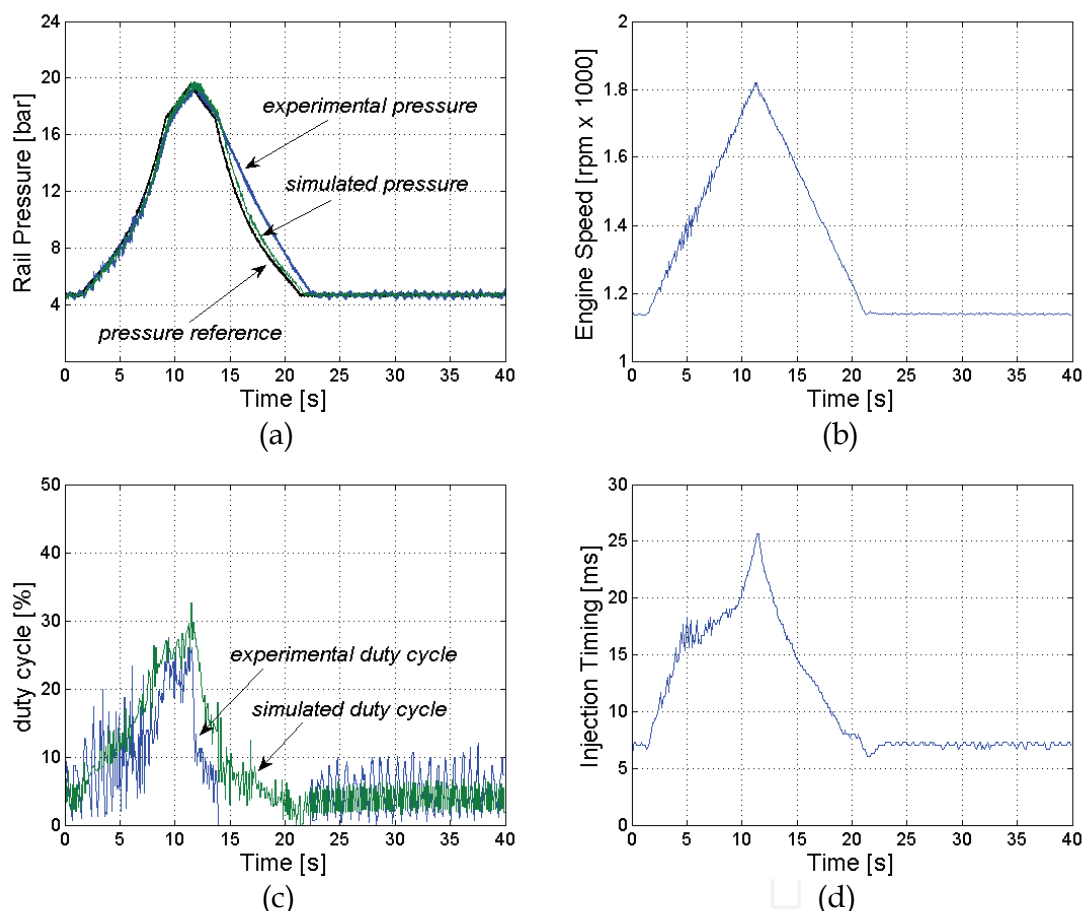

Fig. 7. Model and real system responses for speed and load ramp variations and a 30bar input pressure, when controlled by a GPC with N = 5; (a) common rail pressure; (b) engine speed (c) *duty cycle*; (d) injectors exciting time interval.

5.2 The diesel injection system

The state space model used for designing the pressure controller has been implemented and simulated in the Matlab/Simulink® environment. To assess its capability of predicting the rail pressure dynamics for each injection cycle, simulation results have been compared both with experimental data obtained on a Common Rail injection system (Dinoi, 2002) and with

those provided by the AMESim software for fluid dynamic simulation. Modelling and simulation within this prototyping environment are used for verifying alternative designs and parameterizations. For the sake of brevity, experimental results are not shown in this chapter (see Lino et al., 2007 for details).
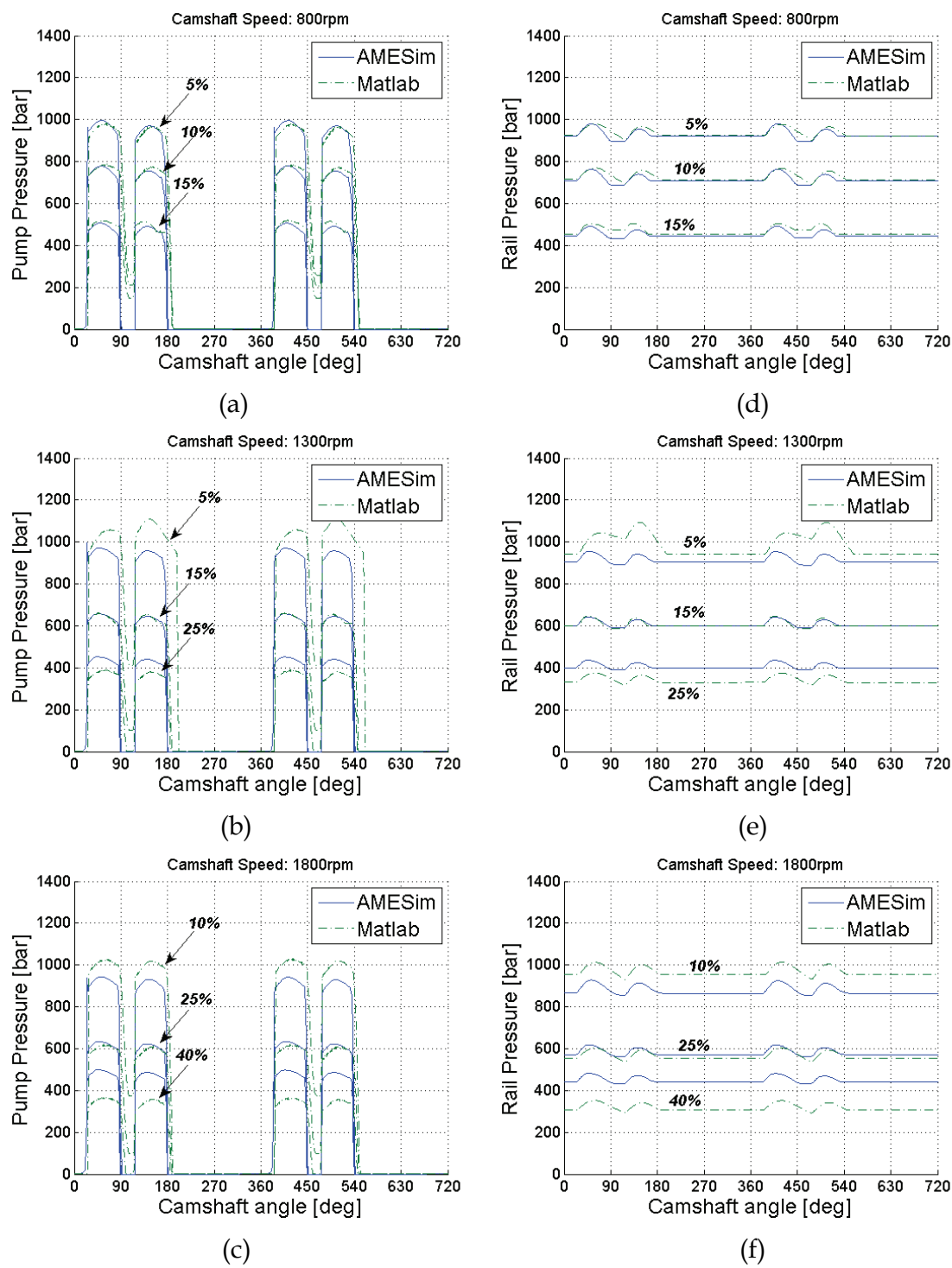

Fig. 8. Comparison of AMESim and Matlab simulated pump and rail pressures, by varying the solenoid valve driving signal and for different camshaft speeds: (a), (b), (c) pump pressure; (d), (e), (f) rail pressure.

Fig. 8 compares Matlab and AMESim simulations referred to two complete camshaft revolutions. This figure represents pump and rail pressures, for 800, 1300 and 1800 rpm camshaft speeds respectively, and different values of the electro-hydraulic valve duty-cycle. According to Figure 8, the pump pressure increases because of the piston motion, until the delivery valve opens. From this moment on, the pressure decreases because of the outflow towards the rail. Subsequently, the pressure increases again because of the camshaft profile. The rail pressure is constant during the angular interval in which the delivery valve is closed. The opening of the delivery valve causes a pressure increase, which is immediately compensated by the intervention of the regulation valve. We can conclude that the pressure dynamics are well modelled, both in amplitude and in timing. The difference in the steady values is due to the approximation introduced in the state space model for the electro-hydraulic valve.
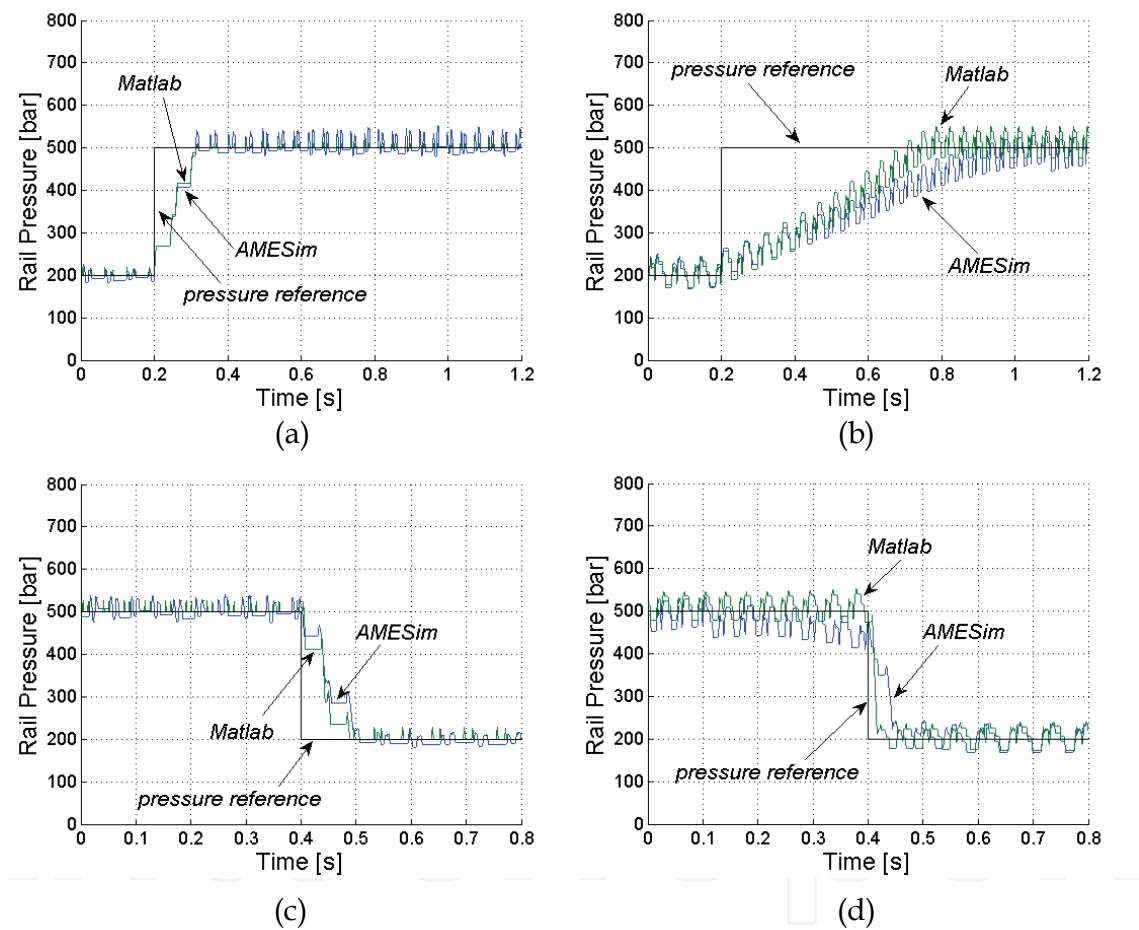

Fig. 9. AMESim and Matlab rail pressure dynamics with reference step variations and ramp camshaft speed variations; (a) step and ramp increments in absence of injections; (b) step and ramp increments in presence of injections; (c) step and ramp decrements in absence of injections; (d) step and ramp decrements in presence of injections.

To test the sliding mode controller tracking and disturbance rejection capabilities we have extensively simulated different operating conditions by using AMESim software. To check the effectiveness of the approach AMESim simulations with Matlab simulations of the state space model have been compared. Significant results are discussed in the following.

First of all, it is considered a reference pressure step variation, by varying the camshaft speed, without injections. In Fig. 9a, a 300 bar set-point variation occurs at time 0.2, starting from 200bar up to 500bar. The initial 1000rpm camshaft speed increases to 1600rpm following a ramp profile, within a 0.5s time interval starting at time 0.2s. The injectors are kept completely closed, so that the controller copes with the pressure disturbances due to the pump motion. Moreover, the control action, computed at the beginning of each injection cycle, is applied during the valve activation window. The rail pressure is properly taken close to the set-point without any overshoot, but it suffers of undesirable oscillations, as the control action is held constant during the whole camshaft revolution. Figure 9b considers analogous operating conditions, but in presence of injections. The injectors' driving signal acts to keep the angular opening interval constant, regardless of the camshaft speed. The sliding mode controller is still able to maintain the rail pressure close to the reference value, with a good rejection of the disturbance due to the injection flow. The high pressure oscillations, due to the injectors' operation, cannot be removed as the control valve acts only during the activation window. Finally, the rising transient is slower than the previous case, as a fraction of the fuel delivered by the pump is sent to cylinders. In both cases, Matlab simulations are in good accordance with those performed within the AMESim environment, showing the feasibility of the derivation of the control law from the reduced order model.

In Figures 9c and 9d, a pressure reference step variation occurs at time 0.4, while the speed decreases from 1600rpm to 1000rpm, within a 0.5s time interval starting at time 0.2s, following a ramp profile. In the first case (Fig. 9c), the injectors are kept completely closed. In the second case (Fig. 9d), the injectors opening time is proportional to the camshaft speed. It is possible to note that, within the time interval 0.2-0.4s, the control action is not able to maintain the rail pressure at set-point, as decreasing the pump speed reduces fuel supply for each camshaft revolution. Even in these working conditions the comparison of Matlab and AMESim results confirms the proposed approach.

7. Conclusion

In this chapter, we presented a procedure for integrating different models and tools for a reliable design, optimization and analysis of a mechatronic system as a whole, encompassing the real process and the control system. The effectiveness of the methodology has been illustrated by introducing two practical case studies involving the CNG injection system and the common rail diesel injection system for internal combustion engines. The design process included the possibility of analyzing different candidate configurations carried out with the help of virtual prototypes developed in the AMESim environment, design and performance evaluation of controllers designed on simpler models of the plants by employing the virtual prototypes, validation of the control laws on the real systems. Simulation and experimental results proved the validity of the approach.

8. References

van Amerongen, J. (2003). Mechatronic design. *Mechatronics*, Vol. 13, pp. 1045-1066, ISSN 0957-4158.

van Amerongen, J. & Breedveld, P. (2003). Modelling of physical systems for the design and control of mechatronic systems. *Annual Reviews in Control*, Vol. 27, pp. 87–117, ISSN 1367-5788.

Bertram, T., Bekes, F., Greul, R., Hanke, O., Ha, C., Hilgert, J., Hiller, M., Ottgen, O., Opgen-Rhein, P., Torlo, M. & Ward, D. (2003). Modelling and simulation for mechatronic design in automotive systems. *Control Engineering Practice*, Vol. 11, pp. 179–190, ISSN 0967-0661.

Dellino, G., Lino, P., Meloni, C. & Rizzo, A. (2007a). Enhanced evolutionary algorithms for multidisciplinary design optimization: a control engineering perspective, In: *Hybrid Evolutionary Algorithms*, Grosan, C., Abraham, A., Ishibuchi H. (Ed.), 39-76, Springer Verlag, ISBN 978-3-540-73296-9, Berlin, Germany.

Dellino, G., Lino, P., Meloni, C. & Rizzo, A. (2007b). Kriging metamodel management in the design optimization of a CNG injection system. To appear on *Mathematics and Computers in Simulation*, ISSN 0378-4754.

Dieterle, W. (2005). Mechatronic systems: automotive applications and modern design methodologies. *Annual Reviews in Control*, Vol. 29, pp. 273-277, ISSN 1367-5788.

Dinoi, A. (2002). *Control issues in common rail diesel injection systems* (In Italian), Master Theses, Bari, Italy.

Ferretti, G., Magnani, G. & Rocco P. (2004). Virtual prototyping of mechatronic systems. *Annual Reviews in Control*, Vol. 28, No 2, pp. 193-206, ISSN 1367-5788.

IMAGINE S.A. (2007). *AMESim Reference Manual rev7*, Roanne.

Isermann, R. (1996a). Modeling and design methodology for mechatronic systems. *IEEE Transactions on Mechatronics*, Vol. 1, No 1, pp. 16-28, ISSN 1083-4435.

Isermann, R. (1996b). On the design and control of mechatronic systems – a survey. *IEEE Transactions on Industrial Electronics*, Vol. 43, No. 1, pp. 4-15, ISSN 0278-0046.

Isermann, R. (2008). Mechatronic systems - Innovative products with embedded control. *Control Engineering Practice*, Vol. 16, pp. 14–29, ISSN 0967-0661.

Khalil, H. K., (2002). *Nonlinear Systems*, Prentice Hall, ISBN 978-0130673893, Upper Saddle River.

Lino, P., Maione, B. & Rizzo, A. (2007). Nonlinear modelling and control of a common rail injection system for diesel engines. *Applied Mathematical Modelling*, Vol. 31, No 9, pp. 1770-1784, ISSN 0307-904X.

Lino, P., Maione, B. & Amorese, C. (2008). Modeling and predictive control of a new injection system for compressed natural gas engines. *Control Engineering Practice*, Vol. 16, No 10, pp. 1216-1230, ISSN 0967-0661.

Maione, B., Lino, P., DeMatthaeis, S., Amorese, C., Manodoro, D. & Ricco, R. (2004). Modeling and control of a compressed natural gas injection system. *WSEAS Transactions on Systems*, Vol. 3, No 5, pp. 2164-2169, ISSN 1109-2777.

Ollero, A., Boverie, S., Goodall, R., Sasiadek, J., Erbe, H. & Zuehlke, D. (2006). Mechatronics, robotics and components for automation and control. *Annual Reviews in Control*, Vol. 30, pp. 41–54, ISSN 1367-5788.

Rossiter, J.A. (2003). *Model-Based Predictive Control: a Practical Approach*, CRC Press, ISBN 978-0849312915, New York.

Smith, M. H. (1999). Towards a more efficient approach to automotive embedded control system development, *Proceedings of IEEE CACSD Conference*, pp. 219-224, ISBN 0-7803-5500-8, Hawaii, USA, August 1999.

Stobart, R., May, A., Challen, B. & Morel, T. (1999). New tools for engine control system development. *Annual Reviews in Control*, Vol. 23, pp. 109–116, ISSN 1367-5788.

Streeter, V., Wylie, K. & Bedford, E. (1998). *Fluid Mechanics*, McGraw-Hill, ISBN 978-0070625372, New York.

Stumpp, G. & Ricco, M. (1996). Common rail – An attractive fuel injection system for passenger car DI diesel engine. *SAE Technical Paper 960870.*

Youcef-Toumi, K. (1996) Modeling, design, and control integration: a necessary step in mechatronics. *IEEE Transactions on Mechatronics*, Vol. 1, No. 1, pp. 29-38, ISSN 1083-4435.

Zucrow, M. & Hoffman J. (1976). *Gas Dynamics*, John Wiley & Sons, ISBN 978-0471984405, New York.

Robotics Automation and Control

Edited by Pavla Pecherkova, Miroslav Flidr and Jindrich Dunik

This book was conceived as a gathering place of new ideas from academia, industry, research and practice in the fields of robotics, automation and control. The aim of the book was to point out interactions among various fields of interests in spite of diversity and narrow specializations which prevail in the current research. The common denominator of all included chapters appears to be a synergy of various specializations. This synergy yields deeper understanding of the treated problems. Each new approach applied to a particular problem can enrich and inspire improvements of already established approaches to the problem.

How to reference

In order to correctly reference this scholarly work, feel free to copy and paste the following:

Paolo Lino and Bruno Maione (2008). Multi-Domain Modelling and Control in Mechatronics: the Case of Common Rail Injection Systems, Robotics Automation and Control, Pavla Pecherkova, Miroslav Flidr and Jindrich Dunik (Ed.), ISBN: 978-953-7619-18-3, InTech, Available from: http://www.intechopen.com/books/robotics_automation_and_control/multi-domain_modelling_and_control_in_mechatronics__the_case_of_common_rail_injection_systems

INTECH
open science | open minds